Power Electronic Systems Laboratory

Multiconductor Cable Modelling for EMI Simulations in Power Electronics

I. Stevanovic,
B. Wunsch,
G. Madonna,
M. Vancu,
S. Skibin

ETH

Eidgenössische Technische Hochschule Zürich
Swiss Federal Institute of Technology Zurich

Multiconductor Cable Modeling for EMI Simulations in Power Electronics

Ivica Stevanović*, Bernhard Wunsch*, Gian-Luigi Madonna*, Mircea-Florian Vancu[†] and Stanislav Skibin*

*ABB Switzerland Ltd., Corporate Research, Segelhofstrasse 1K, CH-5405 Baden-Dättwil, Switzerland

Email: ivica.stevanovic@ch.abb.com

[†]Power Electronic Systems Laboratory, ETH Zürich, Physikstrasse 3, CH-8092 Zürich, Switzerland

Abstract—**Reliable simulations of electromagnetic interference (EMI) in power electronic systems ask for accurate models of long power electronic cables. A methodology for creating frequency dependent circuit models of long cables is presented in this paper. It is based on the techniques developed and used for modeling VLSI interconnects and PCB transmission lines in packaging and microwave engineering. A measurement procedure for characterizing experimentally the power cables is explained in detail. Stable, causal, and passive equivalent circuits are then extracted and verified by comparing the simulation results with frequency- and time-domain measurements.**

I. Introduction

Power electronic converters are used in many industrial applications including energy generation and motor drives among others. The main source of electromagnetic interference (EMI) in power converters is fast switching of semiconductor devices, where steep voltage and current slopes introduce high-frequency disturbances in the system, known as common mode (CM) and differential mode (DM) emissions. These emissions travel and spread over the power electronic system via low resistive and inductive interconnects such as power cables [1].

In order to have reliable prediction of EMI in power electronic systems, accurate models of all the components in the path of CM and DM noise propagation are necessary. Special care needs to be taken when modeling longer power cables; they need to be treated as distributed multiconductor transmission lines where many frequency dependent phenomena such as skin and proximity effects, dielectric losses, and delay need to be properly taken into account [2].

Power electronic cables are typically modeled using a lumped version of the telegraph equations, where per-unit-length (p.u.l.) parameters are either measured [3], [4], analytically predicted [5], [6], or simulated using electromagnetic full wave solvers [4]. Direct measurement of the p.u.l. parameters at different frequencies is a complicated procedure and may lead to inaccurate results. In many electromagnetic solvers the p.u.l. parameters are extracted at a given frequency and as constant values used to create an equivalent circuit. It has been shown that neglecting the information on frequency dependency of characteristic impedance and propagation losses leads to inaccurate results. Analytical formulas on the other hand are approximate and available only for a few canonical geometries of cable conductors' cross sections. The above mentioned techniques have been used for rather short cables, up to $20\,\mathrm{m}$ in length.

Frequency dependent modeling of interconnects in VLSI and microwave circuits has been a subject of active research [2]. The methods developed there for modeling of interconnects (usually printed board transmission lines) can be roughly classified in two different groups: based on p.u.l. parameters obtained using rigorous full-wave electromagnetic simulations [7], [8] or based on port response at discrete frequency points in form of scattering parameters (measured or simulated) [9]–[11].

In this work, we adopt the latter approach and apply it to modeling of longer power cables. In a first step we measure the port parameters of the cable in the conducted emission EMI frequency band including DC point; then we fit the measured values by a continuous rational function ensuring stable, causal, and passive models [12]; and finally create an equivalent circuit using Laplace elements that can be used in SPICE time and frequency domain circuit simulations. The resulting models embody all the frequency dependent phenomena of the measured cable. The method has been validated using frequency and time domain measurements on a $150\,\mathrm{m}$ long, shielded, 3-conductor power cable. The models show an excellent agreement with measurements and prove to be passive and stable in large circuit-level EMI simulations.

II. Cable Measurements

Assume the cable is a multiconductor transmission line with a total of $n+1$ conductors. The first n conductors are referred to as the signal conductors. The last conductor (usually the shield in a shielded power cable) is referred to as the reference (or ground) conductor. A port is defined between each signal conductor and the reference conductor at near and far ends of the cable. The cable with $n+1$ conductors can then be represented as a linear, passive electrical network with a total of $2n$ ports. Figure 1 shows the notation for the port numbering, where the ith signal conductor is assumed to be between port i and port $i+n$.

A multiport network can be completely described by its admittance matrix that relates the currents and voltages at the ports (see Fig. 1(a)):

$$\begin{bmatrix} i_1 \\ \vdots \\ i_{2n} \end{bmatrix} = \begin{bmatrix} y_{1,1} & \cdots & y_{1,2n} \\ \vdots & \ddots & \vdots \\ y_{2n,1} & \cdots & y_{2n,2n} \end{bmatrix} \begin{bmatrix} v_1 \\ \vdots \\ v_{2n} \end{bmatrix} \qquad (1)$$

or in the equivalent matrix notation

$$\mathbf{I} = \mathbf{YV}. \qquad (2)$$

The admittance matrix $\mathbf{Y}$ can be measured by placing a voltage source at one port at a time, short-circuiting all the other ports, and measuring the currents that flow in all the ports. Although this may be accurately done at DC, measuring the $\mathbf{Y}$ matrix at higher frequencies is significantly more difficult since short-circuit conditions are not simply met.

Instead of port voltages and currents, traveling waves are often preferred at high frequency. The incident traveling wave at port i of the network in Fig. 1(b) is defined as a linear combination of voltage and current at the same port [13]

$$a_i = \frac{v_i + Z_{0i}i_i}{2\sqrt{Z_{0i}}} \qquad (3)$$

where Z_{0i} is the reference impedance for port i, assumed to be a real number. In many practical cases, the reference impedance is chosen equal to $50\,\Omega$. Similarly, the reflected traveling wave at port i is defined as

$$b_i = \frac{v_i - Z_{0i}i_i}{2\sqrt{Z_{0i}}}. \qquad (4)$$

These quantities are related by the scattering matrix $\mathbf{S}$:

$$\begin{bmatrix} b_1 \\ \vdots \\ b_{2n} \end{bmatrix} = \begin{bmatrix} s_{1,1} & \cdots & s_{1,2n} \\ \vdots & \ddots & \vdots \\ s_{2n,1} & \cdots & s_{2n,2n} \end{bmatrix} \begin{bmatrix} a_1 \\ \vdots \\ a_{2n} \end{bmatrix} \qquad (5)$$

The scattering parameter s_{ii} represents the reflection coefficient at port i when all the other ports are terminated by the reference impedance, whereas the parameter s_{ij} is the transmission coefficient from port j to port i in the same conditions. Given the relations (3) and (4), if either of the two matrices are known, the other matrix is then obtained using the following algebraic transformation [14], [15]

$$\mathbf{S} = \left(\mathbf{G}^{-1} + \mathbf{YG}\right)^{-1}\left(\mathbf{G}^{-1} - \mathbf{YG}\right) \qquad (6)$$

$$\mathbf{Y} = \mathbf{G}^{-1}\left(\mathbf{1} + \mathbf{S}\right)^{-1}\left(\mathbf{1} - \mathbf{S}\right)\mathbf{G}^{-1} \qquad (7)$$

where $\mathbf{G}$ is a diagonal matrix whose ith component is given by $\sqrt{Z_{0i}}$. In case $Z_{0i} = Z_0$ for all the ports, the above relations are simplified and given by

$$\mathbf{S} = \left(\mathbf{1} + Z_0\mathbf{Y}\right)^{-1}\left(\mathbf{1} - Z_0\mathbf{Y}\right) \qquad (8)$$

$$\mathbf{Y} = \frac{1}{Z_0}\left(\mathbf{1} + \mathbf{S}\right)^{-1}\left(\mathbf{1} - \mathbf{S}\right) \qquad (9)$$

where $\mathbf{1}$ is a unity matrix of dimension $2n$.

The s-parameter matrix can be rigorously measured by a multiport vector network analyzer (VNA). Since the availability of this equipment is not widely spread, a more traditional two-port VNA can be used instead; the entire $\mathbf{S}$ matrix is then measured by connecting alternating couples of the cable ports to the instrument, while terminating all the remaining ones by the chosen reference impedance. In particular, a two-port VNA connection between port i and j gives the $\mathbf{S}$-matrix elements s_{ii}, s_{ij}, s_{ji} and s_{jj} (provided that all the remaining ports are
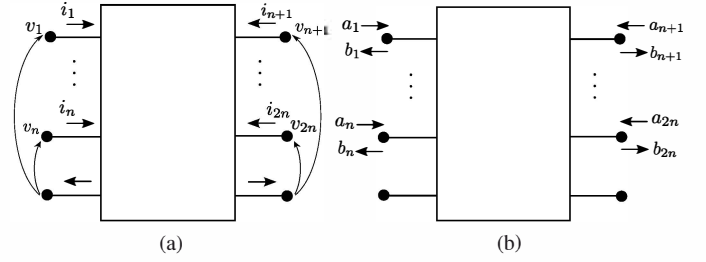

Fig. 1: Description of cable as a multiport network. (a) The admittance matrix relates voltages between signal conductors and shield (reference conductor) to the currents entering the signal conductors. (b) The s-parameter matrix relates incoming and outgoing waves at the ports defined by each signal conductor and the reference conductor.

terminated by the reference impedance). This has proven to provide an accuracy sufficient for our purposes, provided that the procedure described in the next section is followed.

A. S-parameter measurements using vector network analyzer

The measurement setup used in characterizing the s parameters of the cables consists of

- Two-port VNA with BNC connectors
- Cable adapters (or fixtures) providing good connection of the cable signal conductors and shielding to the BNC connectors of the VNA
- Calibration kit (consisting of open, short, $50\,\Omega$ load and thru) for removing the systematic errors due to the cable fixtures and (in general) for the network analyzer calibration.

The fixtures and calibration kits need to be designed for each cable type and depend on the number of conductors, geometry of the conductors, as well as on the way the cable will be connected to the system in operation. One example of the fixtures and calibration kit we used for measuring a shielded three conductor power cable is shown in Fig. 2. The cable shielding is mechanically connected to the fixture connectors via screws and no soldering is necessary. There are two types of fixtures, one for each end of the cable and they have the same connectors used to connect the cable between the motor drive (Fig. 2(a)-(b)) and the motor (Fig. 2(c)-(d)) and thereby allow us to include the effect of the connectors and the conductor pigtails into the model. This type of fixture is general since cables with up to four signal conductors and with different geometries can be measured.

The s parameters were measured in the frequency range from $9\,\text{kHz}$ (minimum operating frequency of the VNA) up to $50\,\text{MHz}$ using a fully calibrated (open-short-load-thru) network analyzer, covering this way the EMI regulated conducted emission range. During the measurements, two cable ports were connected to the VNA, while all the remaining ports were terminated using $50\,\Omega$ BNC loads. Starting from the $\mathbf{S}$

matrix and using the transformation given in (9) we can obtain the values of the corresponding $\mathbf{Y}$ matrix.
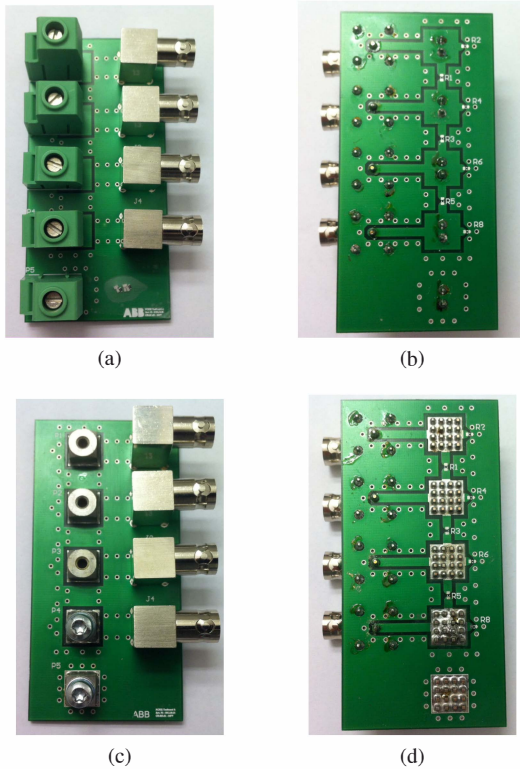
(a)

(b)

(c)

(d)

Fig. 2: Fixtures that can be used to measure three and four conductor shielded power cables take into account the way the cable is in practice connected to the motor drive (a,b) and to the motor (c,d).

B. Symmetric properties of the Y matrix

Due to the reciprocity, the following property holds for the y-parameter (or equivalently s-parameter) matrix: $y_{ij} = y_{ji}$, $j \neq i$. Therefore, only the y parameters on the main diagonal and in the lower (or upper) triangle submatrix can be considered. In addition, due to the symmetry present in the cable's geometry, one can group the y parameters of a three conductor cable according to the following rules (see Fig. 3):

- Self admittance of the ports $y_{11} = y_{22} = \ldots = y_{66}$
- Mutual admittance between the ports that are galvanically connected but belong to the opposite ends $y_{14} = y_{25} = y_{36}$
- Mutual admittance between the ports that are neighbors and belong to the same end $y_{12} = y_{23} = y_{31} = y_{45} = y_{56} = y_{46}$
- Mutual admittance between the ports that are neighbors and belong to the opposite ends $y_{15} = y_{26} = y_{34} = y_{16} = y_{35} = y_{24}$.

If the cable geometry is symmetric, distinct groups of parameters should be clearly visible in the measurements: 4 different groups at higher frequencies for a three conductor cable with very small spread within each group (Fig. 4), and two different

groups of parameters at low frequencies. The distribution of resonances in the measured y parameters is very close to linear and there is a visible damping in the resonance peaks as the frequency increases.
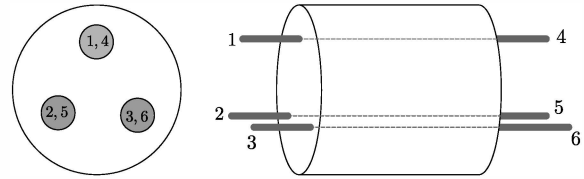
Fig. 3: Grouping the y parameters for three conductor cable according to the symmetry and reciprocity.
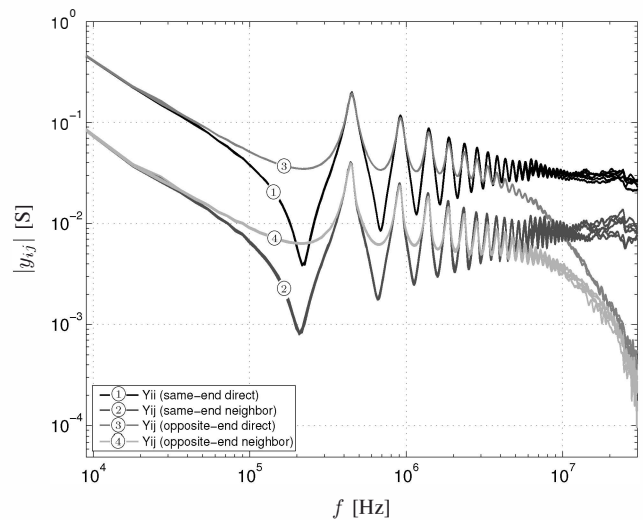
Fig. 4: Measured y parameters of the $150\,\mathrm{m}$ shielded three conductor cable.

C. DC Measurements

Using the VNA, the minimum frequency measured is in the lower kHz range. In order to create a model of the cable that predicts correctly the DC behavior, we need to perform the measurements at DC. For that purpose, we used a simple multimeter and measured the resistances of the signal and shield conductors between the far ends of the cable.

Let the measured resistance of each signal conductor at DC be R and that one of the braided shielding R_{sh}. At DC there is no inductive or capacitive coupling between the conductors and the equivalent circuit of a shielded three conductor cable can then be represented as in Fig. 5. In order to avoid any convergence issues, and to increase the stability margin of the model within circuit simulators, we have introduced large shunt resistors R_{G} between each signal conductor and the reference conductor as shown in the same figure (as without them the $\mathbf{Y}$ matrix of the circuit would be singular). The $\mathbf{Y}$ matrix of this circuit network for a shielded cable with n signal conductors can be represented using the following expressions
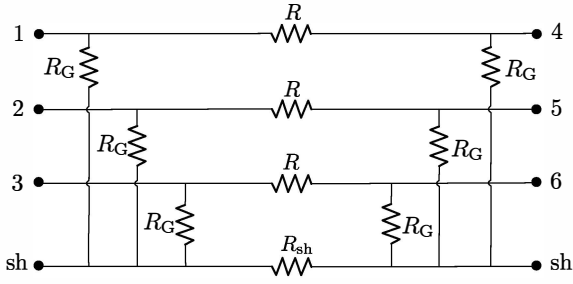
Fig. 5: Circuit model of a shielded three conductor cable at DC with non-singular $\mathbf{Y}$ matrix.

$$\mathbf{Y}_{\text{dc}} = \begin{bmatrix} \mathbf{Y}_{\text{i}} & \mathbf{Y}_{\text{t}} \\ \mathbf{Y}_{\text{t}} & \mathbf{Y}_{\text{i}} \end{bmatrix} \tag{10}$$

where

$$\mathbf{Y}_{\text{i}} = \begin{bmatrix} y_{\text{s}} & y_{\text{m1}} & \cdots & y_{\text{m1}} \\ y_{\text{m1}} & y_{\text{s}} & \cdots & y_{\text{m1}} \\ \vdots & \vdots & \ddots & \vdots \\ y_{\text{m1}} & y_{\text{m1}} & \cdots & y_{\text{s}} \end{bmatrix}_{n \times n} \tag{11}$$

$$\mathbf{Y}_{\text{t}} = \begin{bmatrix} y_{\text{m2}} & -y_{\text{m1}} & \cdots & -y_{\text{m1}} \\ -y_{\text{m1}} & y_{\text{m2}} & \cdots & -y_{\text{m1}} \\ \vdots & \vdots & \ddots & \vdots \\ -y_{\text{m1}} & -y_{\text{m1}} & \cdots & y_{\text{m2}} \end{bmatrix}_{n \times n} \tag{12}$$

and

$$y_{\text{s}} = \frac{1}{R_{\text{G}}} + \frac{1}{R + \frac{1}{\frac{n-1}{R} + \frac{1}{R_{\text{sh}}}}} \tag{13}$$

$$y_{\text{m2}} = -\frac{1}{R + \frac{1}{\frac{n-1}{R} + \frac{1}{R_{\text{sh}}}}} \tag{14}$$

$$y_{\text{m1}} = \frac{1}{n - 1 + \frac{R}{R_{\text{sh}}}} \frac{1}{R + \frac{1}{\frac{n-1}{R} + \frac{1}{R_{\text{sh}}}}}. \tag{15}$$

The matrix $\mathbf{Y}_{\text{dc}}$ is then added to the tabulated data consisting of measured $\mathbf{Y}$ matrices at higher frequencies.

III. RATIONAL FUNCTION FITTING OF TABULATED DATA

Once the frequency-dependent measured $\mathbf{Y}$ matrix is available for a given cable at a given set of discrete frequencies f_k, the first step in creating the equivalent circuit of the cable is to fit a continuous rational matrix function to the measurements. The fitted rational function $\mathbf{Y}(s)$ is an analytical function of the complex variable s (except for a set of poles s_i) and can be represented in a pole-residue form as

$$\mathbf{Y}(s) = \sum_{i=1}^{N_{\text{p}}} \frac{\mathbf{R}_i}{s - s_i} + \mathbf{D} \tag{16}$$

where s_i are poles, $\mathbf{R}_i$ are residue matrices, and $\mathbf{D}$ describes the infinite frequency limit of the admittance matrix. Note that $\mathbf{Y}(s)$, $s = \text{j}2\pi f$ determines the admittance matrix at all frequencies f, and not only at the measured frequencies f_k.

The unknown coefficients s_i and $\mathbf{R}_i$ can be calculated using different complex curve fitting procedures. Gustavsen Vector Fitting Toolbox [12], [16] is used in this work. The Gustavsen approach ensures that the final rational function approximation is

- Causal (the admittance matrix is real for real values of s meaning that s_i and $\mathbf{R}_i$ are either both real or they occur in complex conjugate pairs.
- Stable (the real part of the poles are negative)
- Passive (the $\mathbf{Y}(\text{j}2\pi f)$ matrix is positive semi-definite)

The number of poles in the vector fitting algorithm determines the complexity of the obtained model. By choosing the lowest number of poles that adequately fit the data in the relevant frequency range, one effectively creates a minimal model for the cable. Vector fitting acts, therefore, as a model order reduction algorithm. Moreover, the vector fitting acts as a frequency filter, since the obtained model will fit the measured data in the frequency range of the measurements while it is a smooth function outside that frequency range. This is an attractive feature for cables that in principles show resonances at all frequencies. High frequency resonances often yield small time steps in the circuit simulations so that the effective high frequency cut-off enables larger time steps and faster simulations.

IV. SPICE EQUIVALENT CIRCUIT REPRESENTATION

The causal, stable, and passive pole-residue representation of the cable has to be translated into an equivalent subcircuit that can be linked to a SPICE circuit solver. That can be done using either generalized π structure [17] or an equivalent circuit based on state-space description [2]. For the SPICE solvers that accept Laplace elements, the former representation is especially well suited and straightforward to implement and we have adopted it in this work.

V. VALIDATION AND VERIFICATION

In this section, we present the results of our numerical simulations and compare them to the time- and frequency-domain measurements, in order to validate the theory presented in this paper. As an example we use a shielded three conductor EMC cable with the signal conductor cross section of $16\,\text{mm}^2$ and of the length of $150\,\text{m}$.

A. Frequency Domain

Using the values measured at DC ($R = 0.1\,\Omega$, $R_{\text{sh}} = 0.07\,\Omega$) and the VNA measured port parameters in the range from $9\,\text{kHz}$ through $30\,\text{MHz}$ we have applied the vector fitting procedure with passivity enforcement using 120 poles with linear distribution. The resulting fitted model has been transformed into a SPICE netlist using Laplace elements. The results of the simulations compare very favorably with measured values for the four different groups of y parameters as shown in Fig. 6.

(a) Self admittance.

(b) Mutual admittance (same end neighbors).

(c) Mutual admittance (opposite ends, direct connection).

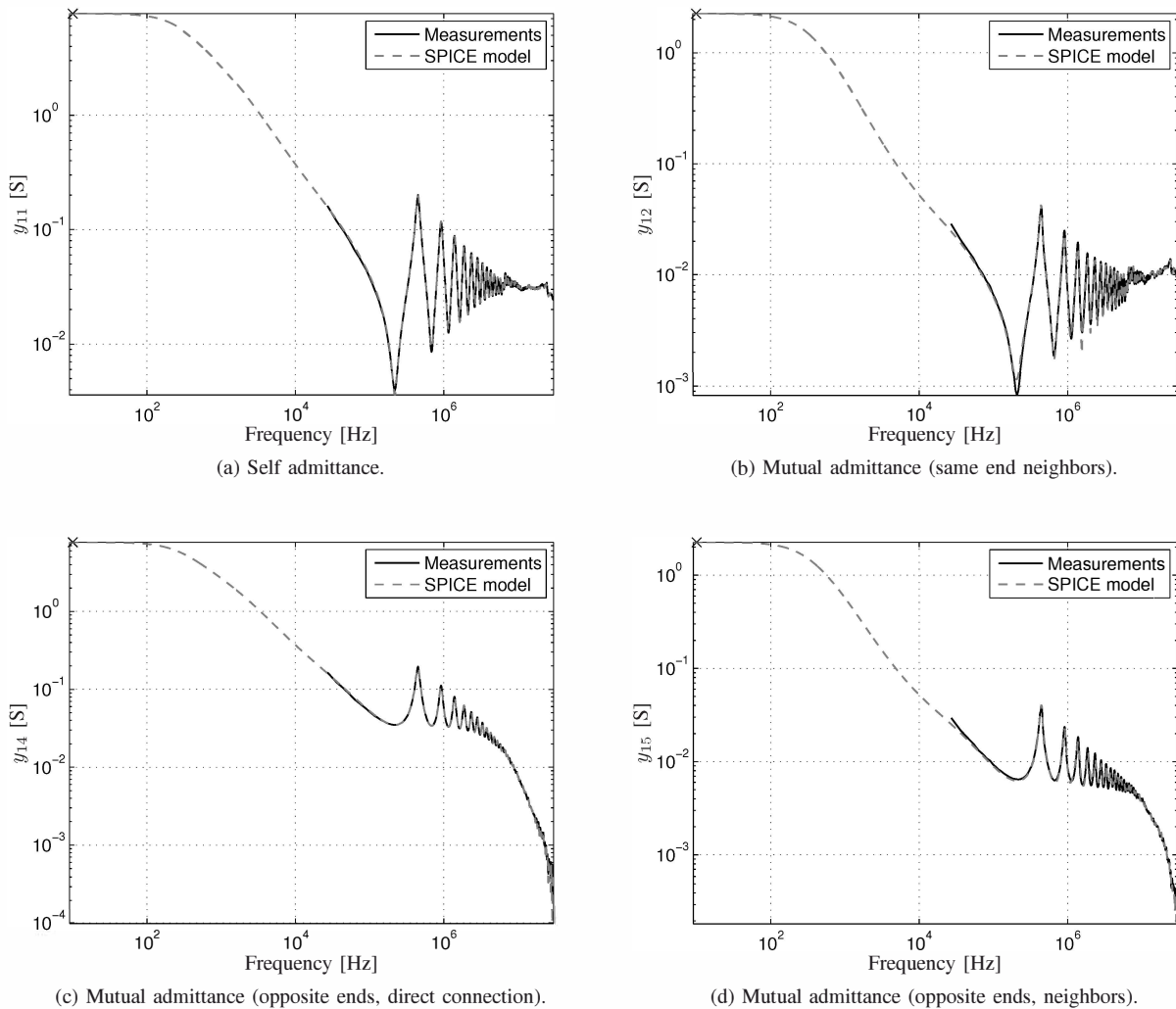

(d) Mutual admittance (opposite ends, neighbors).

Fig. 6: Admittance of the 150 m three conductor shielded cable: measurements (solid lines), simulations (dashed lines), measured DC ($\times$ symbol).

B. Time Domain

In this subsection we compare the time domain simulations with measured data. The simulation is based on the equivalent circuit derived in previous section. The measurement setup is schematically illustrated in Fig. 7. The setup consists of a signal generator, current probes, and high-frequency voltage probes used to measure current and voltage waveforms. The signal generator is connected between two signal conductors at the near end of the cable. The input voltage from the signal generator is a periodic trapezoidal train of pulses with period $5\,\mu s$, a width of $2.5\,\mu s$, and with equal rise and fall time $25\,ns$. At the far end of the cable, the two signal conductors are connected over a resistor $R = 102\,\Omega$. At the near end, the shielding is connected to the return path signal conductor. We measured the voltage between the two signal conductors at the near end V_{in}, the current at the far end of the cable I_{out}, and the crosstalk current in the shielding I_{sh} (the braided shielding at the far end of the cable is left floating). This setup is simulated using the cable model developed in this work and the simulated results are in very good agreement with measurements as shown in Fig. 8.
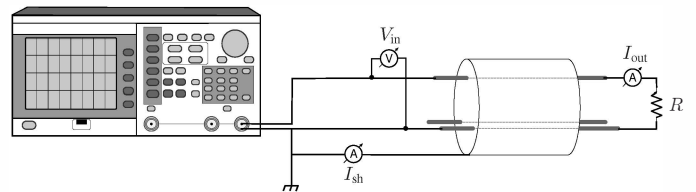

Fig. 7: Schematic setup for the time domain measurements.

VI. CONCLUSION

In this paper, we have presented and benchmarked a consistent and self-contained methodology for creating frequency
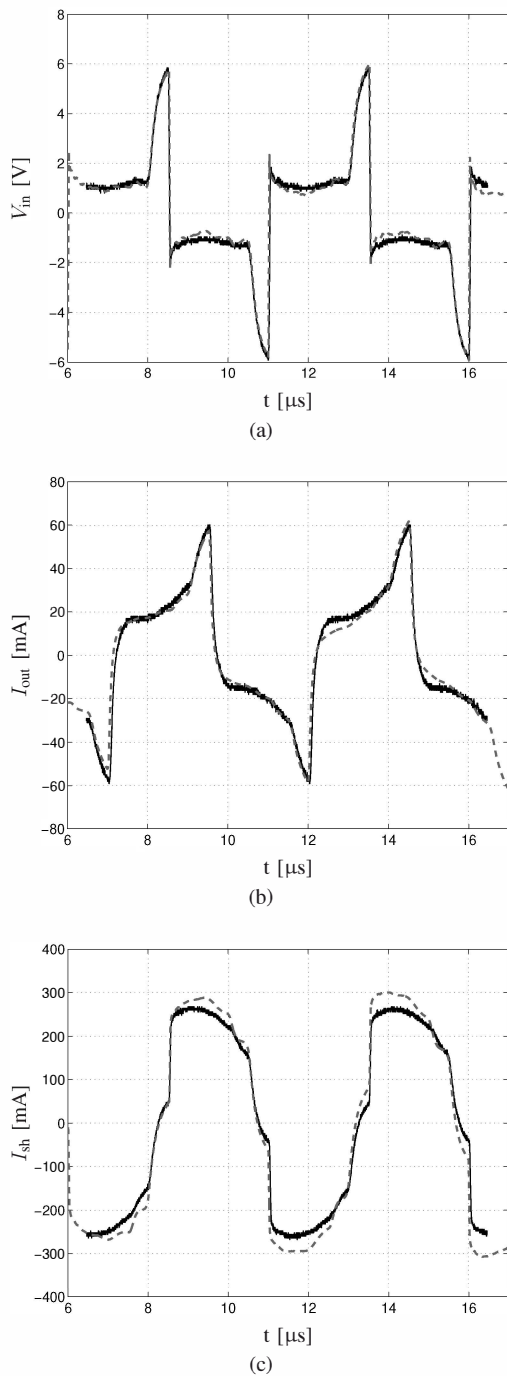
Fig. 8: Comparison between simulation (dashed lines) and measurements (solid lines) of the circuit shown in Fig. 7.

dependent circuit models of long cables used in power electronic systems. The methodology is based on the techniques developed and used for modeling VLSI interconnects and printed board transmission lines in packaging and microwave engineering, where tabulated port parameters are fit with rational functions. The tabulated port parameters of the cable are obtained using a combination of vector network analyzer and DC measurements. For the former, we have designed

and manufactured fixtures and a calibration kit, that allow deembedding the port parameters from measurements of power cables with up to four signal conductors and different conductor cross sections. For the latter, we have devised a procedure for including the DC y parameters to the VNA measured higher frequency tabulated port parameters. Stable, causal, and passive equivalent circuits are extracted and represented in SPICE netlists in the form of Laplace elements. The methodology has been verified and validated on several different power cables. An example with a $150\,\mathrm{m}$ three conductor shielded power cable has been presented in this paper and the results of simulations show good agreement with both time and frequency domain measurements.

REFERENCES

[1] S. Pignari and A. Orlandi, "Long-cable effects on conducted emissions levels," *IEEE Trans. Electromagn. Compat.*, vol. 45, no. 1, pp. 43 – 54, feb 2003.
[2] R. Achar and M. Nakhla, "Simulation of high-speed interconnects," *Proc. IEEE*, vol. 89, no. 5, pp. 693–728, May 2001.
[3] Y. Weens, N. Idir, R. Bausière, and J. J. Fanchaud, "Modeling and simulation of unshielded and shielded energy cables in frequency and time domains," *IEEE Trans. Magn.*, vol. 42, no. 7, pp. 1876–1882, Jul. 2006.
[4] N. Idir, Y. Weeens, and J.-J. Franchaud, "Skin effect and dielectric loss models of power cables," *IEEE Trans. Dielectr. Electr. Insul.*, vol. 16, no. 1, pp. 147–154, Feb. 2009.
[5] J. Dickinson and P. J. Nicholson, "Calculating the high frequency transmission line parameters of power cables," in *1st Int. Symp. Power-Line Communications and its Applications (ISPLC 97)*, Apr. 1997, pp. 127–133.
[6] Y. Tanji and A. Ushida, "Closed-form expression of RLCG transmission lie and its application," *Electronics and Communications in Japan (Part III: Fundamental Electronic Science)*, vol. 87, no. 4, pp. 1–11, Apr. 2004.
[7] A. Djordjevic, "SPICE-compatible models for multiconductor transmission lines in Laplace-transform domain," *IEEE Trans. Microw. Theory Tech.*, vol. 45, no. 5, pp. 569–579, May 1997.
[8] A. Dounavis and V. Pothiwala, "Passive closed-form transmission line macromodel using method of characteristics," *IEEE Trans. Adv. Packag.*, vol. 31, no. 1, pp. 190–202, Feb. 2008.
[9] R. Neumayer, F. Haslinger, A. Stelzer, and R. Weigel, "Synthesis of SPICE-compatible broadband electrical models from n-port scattering parameter data," in *IEEE Int. Symp. on Electromagnetic Compatibility*, vol. 1, Minneapolis, MN, Aug. 19-23, 2002, pp. 469–474.
[10] D. Saraswat, R. Achar, and M. Nakhla, "A fast algorithm and practical considerations for passive macromodeling of measured/simulated data," *IEEE Trans. Adv. Packag.*, vol. 27, no. 1, pp. 57–70, Feb. 2004.
[11] A. Chinea, P. Triverio, and S. Grivet-Talocia, "Delay-based macromodeling of long interconnects from frequency-domain terminal responses," *IEEE Trans. Adv. Packag.*, vol. 33, no. 1, pp. 246–256, Feb. 2010.
[12] B. Gustavsen, "Computer code for passivity enforcement of rational macromodels by residue perturbation," *IEEE Trans. Adv. Packag.*, vol. 30, no. 2, pp. 209–215, May 2007.
[13] A. R. Djordjevic, D. D. Cvetkovic, G. M. Cujic, T. K. Sarkar, and M. B. Bazdar, *MULTILIN for Windows: Circuit-Analysis Models for Multiconductor Transmission Lines, Software and User's Manual.* Norwood, MA: Artech House, 1996, ch. 5: Multiconductor Transmission Line Theory, pp. 51–84.
[14] K. Kurokawa, "Power waves and the scattering matrix," *IEEE Trans. Microw. Theory Tech.*, vol. 13, no. 2, pp. 194–202, Mar. 1965.
[15] P. Russer, *Electromagnetics, Microwave Circuit and Antenna Design for Communications Engineering.* Norwood, MA: Artech House, 2003.
[16] B. Gustavsen, "Fast passivity enforcement for pole-residue models by perturbation of residue matrix eigenvalues," *IEEE Trans. Power Del.*, vol. 23, no. 4, pp. 2278–2285, Oct. 2008.
[17] A. S. Morched, J. H. Ottevangers, and L. Marti, "Multi-port frequency dependent network equivalents for the EMTP," *IEEE Trans. Power Del.*, vol. 8, no. 3, pp. 1402–1412, Jul. 1993.